Slov Vet Res 2015; 52 (2): 75-85
UDC 577.352:546.26:612.111:636.7

Original Scientific Article

EFFECT OF CARBON BLACK NANOMATERIAL ON CANINE ERYTHROCYTE AND PLATELET SHAPE

Judita Lea Krek[1], Metka Šimundić[3], Mitja Drab[1], Manca Pajnič[1], Vid Šuštar[4], Roman Štukelj[1], Damjana Drobne[2], Veronika Kralj-Iglič[1]

[1]Laboratory of Clinical Biophysics, Faculty of Health Sciences, University of Ljubljana, Zdravstvena pot 5; [2]Group of Nanobiology and Nanotoxicology, Department of Biology, University of Ljubljana, Večna pot 111; [3]Prva Clinics for Small Animals, Gorkičeva 6, 1000 Ljubljana, Slovenija, [4]Lymphocyte Cytoskeleton Group, Department of Pathology, University of Turku, Medical Faculty, Tykistökatu 6B, FIN-20520 Turku, Finland

*Corresponding author, E-mail: veronika.kralj-iglic@fe.uni-lj.si

Summary: The effect of carbon black agglomerated nanomaterial on biophysical properties of canine red blood cell and platelet membranes that are reflected in changes of cell shape, was studied. Samples of canine blood diluted with citrated and phosphate buffered saline were incubated with carbon black nanomaterial and observed by scanning electron microscope and optical microscope. Interaction of agglomerated nanomaterial with erythrocyte membrane was observed. The relative abundance of different erythrocyte shape types (discocytes, echinocytes, spherically shaped erythrocytes) was determined on populations of cells, in suspensions with added carbon black nanomaterial and in control suspensions. Ensembles composed of representative images of cell populations were assessed by statistical methods. A two dimensional mathematical model of the erythrocyte shape was constructed to illustrate and explain erythrocyte swelling of intially discocytic/echinocytic shape to the final spherical shape, which preceeds membrane rupture. Micrometre-sized agglomerates were formed in the blood and interacted with erythrocyte membrane without evidently disturbing local membrane curvature or global cell shape. Incubation of blood with citrated and phosphate buffered saline caused a time dependent decrease of the number of intact erythrocytes in samples that was ascribed to a disintegration of erythrocyte membranes. The presence of carbon black nanomaterial in the samples suppressed this effect. Relative proportions of cell shape types remained largely unchanged within 24 hours of observation of the test and the control sample. The observed effects of carbon black nanomaterial can be described as originating from osmosis. Incubation of canine platelets with carbon black nanomaterial within 24 hours preserved the disc-like shape that is characteristic for resting platelets. It was concluded that carbon black nanomaterial interacts with membranes of blood cells but does not have a direct effect on the local or global membrane shape. However, large size of carbon black agglomerates, that can be formed in blood plasma could present mechanical obstacles in the cardiovascular system.

Key words: carbon black; nanoparticles; erythrocyte shape; osmosis; nanomaterial safety; nanotoxicology; alternatives to laboratory / experimental animals

Introduction

Environmental pollution is a subject of increasing interest due to its potentially harmful effect on the health of human (1-4) and animals (5-8). Carbon black (CB) is produced by the incomplete combustion of petroleum products, such as in traffic. When inhaled, small enough particles of CB can enter the circulation and in this way also reach the tissue cells. The adverse effects of CB on health were observed (9-11) while for scientific and medical purposes, the possible mechanisms were studied in vitro (12-15) and in vivo (15). Studies on experimental animals have shown changes in development, in the immune response and in gene expression (15), however, mechanisms underlying harmful effects of CB

Received: 25 July 2014
Accepted for publication: 6 February 2015

on human and animals are yet obscure. Some authors report that the effects of nanomaterial depends primarily on the shape and size of nanoparticles, rather than on their composition (16). This suggests, that non-specific biophysical mechanisms are relevant to describe the effect of nanoparticles on cells and should therefore be included in analyses of the effects of nanomaterial on cells and organisms.

By choosing an appropriate experimental system, the relevant conditions can be achieved and higher standard ethical principles applied in human and in animals (17). Studying basic biophysical mechanisms including the interaction of the test compound with blood cells requires a minimally invasive procedure (taking a small volume of blood) and no material that impairs health and well being of animals. In this work, the in vitro effect of CB on biophysical properties of canine erythrocyte and platelet membranes were considered. As mature mammalian erythrocytes have no internal structure, exogenously added particles that interact with the membrane can cause changes in its properties which is revealed in the change of cell shape (13,21-26). The equilibrium shape of erythrocyte is determined solely by the minimum of the membrane free energy (18,19). Shape changes and mediated interactions are relevant also for platelets, especially since they indicate a propensity of platelets for disturbances in blood clotting that may lead to thromboembolisms (20). It is the aim of this work to consider the effect of carbon black nanomaterial on biophysical properties of biological membranes, that can be deduced from the observed shape changes of erythrocytes and platelets.

Material and methods

Carbon black nanomaterial and suspensions

Nanopowder of CB was purchased from PlasmaChem GmbH (Berlin, Germany) with the average size of primary particles of 13 nm. For experiments with diluted blood samples, washed erythrocytes or platelet rich plasma, stock suspensions of 5 mg/mL CB were prepared in citrated and phosphate buffered saline (PBS): 137 mM NaCl, 2.7 mM KCl, 10 mM $Na_2HPO_4x2H_2O$, 2 mM KH_2PO_4, 10.9 mM $Na_3C_6H_5O_7$. The final concentration of CB in the sample was 1 mg/ml (26).

Blood sampling

The procedures conformed to the European Union's legislation and were in accordance with guidelines set by the Committee for Research and Ethical Issues of IASP. Sampling was performed according to the Declaration of Helsinki and a written informed consent to take blood was given by the animal owners. Blood was taken from two healthy middle-sized pet dogs for which the sample volume represented about 1% of total blood volume. The study was approved by the National Ethics Committee, No 117/02/10. No adverse effects on animals' health due to sampling were observed.

For SEM imaging 10 mL of blood was collected from two healthy dogs (female, 2 years, 13 kg and male, 12 years, 11 kg) into 2.7 mL tubes containing 270 μL trisodium citrate at a concentration 0.109 mol/L (BD Vacutainers, Becton Dickinson, CA). Blood was collected by vein puncture by using a 21-gauge needle (length 70 mm, inner radius 0.4 mm) (Microlance, Becton Dickinson, NJ, USA). Blood was pulled by a syringe.

For direct observation under the optical microscope, 1 mL of blood was collected from a healthy dog (female, 6 years) as described above into a plastic tube without anticoagulant. A drop of blood was taken from the collecting tube immediately after the sampling with a pipette, inserted into an Eppendorf tube previously filled with 1 mL of PBS and gently mixed by turning the sample upside down.

Preparation of blood cells for electron microscopy

Blood was processed within 1 hour from sampling according to previously used protocols (27,13). Blood was centrifuged in a Centric 400R centrifuge (Domel d.o.o., Železniki, Slovenia) at 50 g and 37°C for 15 minutes to separate erythrocytes from platelet rich plasma. Erythrocytes were repeatedly washed with PBS citrate by centrifugation at 1550 g and 37°C for 10 minutes. Washed erythrocytes or platelet rich plasma were aliquoted into equal parts (50 μL in case of erythrocytes and 200 μL in case of platelet rich

plasma). CB suspended in PBS-citrate (or PBS-citrate alone for control) was added to aliquotes in v/v ratio of 2:1 in case of erythrocytes and 3:1 in case of platelet rich plasma, 3 and 2 units corresponding to erythrocytes and platelet rich plasma, respectively. After incubation for 1 hour, the samples were fixed in 0.1% glutaraldehyde, incubated for another hour at room temperature and centrifuged at 1550 g and 37°C for 10 minutes to allow erythrocytes to weakly agglomerate (in order to keep them grouped in pellet for further processing). Supernatant was exchanged for PBS-citrate, samples were resuspended and fixed in 2% glutaraldehyde for an hour at room temperature.

Scanning electron microscopy of blood cells

Fixed samples were washed by exchanging supernatant with citrated PBS and incubated for 20 minutes at room temperature. This procedure was repeated 4 times while the last incubation was performed over night at 8 °C. Samples were then post-fixed for 60 min at 22 °C in 1% OsO_4 dissolved in 0.9% NaCl, dehydrated in a graded series of acetone/water (50%-100%, v/v), critical-point dried, gold-sputtered, and examined using a LEO Gemini 1530 (LEO, Oberkochen, Germany) scanning electron microscope.

Population study of CB effect on erythrocyte shape

PBS-diluted blood samples incubated with the test or control solution were observed under the Leitz Aristoplan (Leitz, Wetzlar, Germany) optical microscope connected to the Watec (Model: 902DM3S), Watec Inc., New York, USA, camera and Pinnacle Studio HD, Version 15.0.0.7593 framegraber and software, Avid Technology Inc., USA. The magnification of the objective was 63 x. The sample was diluted to obtain a density of blood cells composing a monolayer with at least 20 cells on the average in a frame. The test sample was composed of 175 mL of diluted blood and 25 mL of suspended nanomaterial while the control sample was composed of 175 mL of diluted blood and 25 mL of PBS. An observation chamber 1.5 x 1 cm^2 was created on the glass by using silicon grease. 40 μL of the test suspension was placed in the observation chamber and closed by gently pressing the cover glass. Care was taken not to leave voids in the grease boundary in order to prevent evaporation of liquid from the observation chamber. For quantitative analysis of the effect of CB NPs on blood cell membranes, at least 50 frames were randomly imaged over the sample. The images were taken 1 hour, 3 hours and 24 hours after placing the samples into the observation chambers. Regions close to the silicon grease were avoided. During the incubation the samples were kept at the room temperature.

Image analysis of erythrocyte populations

Diluted blood samples contained mostly erythrocytes and singular leukocytes. Leukocytes were not considered. For each sample an ensemble of pictures was created in which we were able to clearly distinguish different possible cell shape types (discocytes, echinocytes, stomatocytes and spherical shapes). The number of intact cells of each shape type was determined in each picture. It was assumed that the pictures were representative for the sample and that the number of cells of each shape type fluctuated around the corresponding average value. The average values of the percent of discocytes, echinocytes, stomatocytes and spherical cells were calculated. 5087 erythrocytes were included in the analysis.

Statistical analysis

The two tailed paired t-test with equal variance to compare the average values was used. Differences with $p<0.05$ were considered statistically significant. Power analysis was performed to validate the size of the samples. Power larger than 0.85 at $\alpha<0.05$ indicated the sample of a proper size. Microsoft Excell software (Microsoft® Office Excel® 2007 SP3) and Power & Sample Size Calculator were used for calculation.

Theoretical model of the cell shape

A two dimensional model of the cell without internal structure was constructed to illustrate the observed shape changes. In the model, the cell membrane was represented by a closed curve with bending but no stretching properties. The curve was described by using polar coordinates (ρ,θ) (Figure 1).

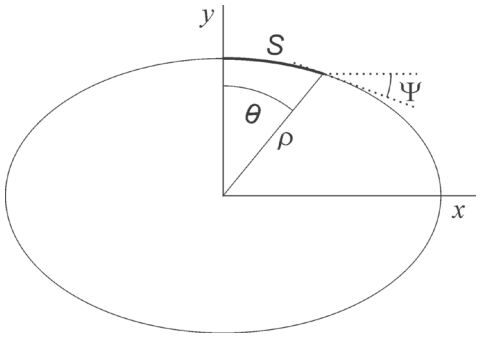

Figure 1: Parametrization of the shape

For convenience, the curve was parametrized by introducing the arclength S and the angle between the tangent to the curve and the x-axis Ψ (Figure 1). The equations of differential geometry give the curvature in terms of the parameters S and Ψ,

$$\dot{\Psi} = C(S), \tag{1}$$

where the dot denotes a derivative with respect to S, $\dot{\Psi} = \mathrm{d}\Psi/\mathrm{d}S$. The bending energy of the curve is given by

$$W_\mathrm{b} = \frac{k_\mathrm{c}}{2}\int_0^L \mathrm{d}S\,(C - C_0)^2, \tag{2}$$

where L is the perimeter of the curve k_c is the two dimensional elastic constant, $\mathrm{d}S$ is the arclength element and C_0 is the spontaneous curvature of the membrane. The spontaneous curvature does not enter the shape equations due to the Gauss-Bonnet theorem. The free energy of the two dimensional erythrocyte is composed of the elastic bending energy and the enthalpic term PA:

$$F = W_\mathrm{b} + PA, \tag{3}$$

where A is the enclosed area and P is the two-dimensional pressure.

Dimensionless quantities are introduced. We define R as a radius of the circle with fixed membrane circumference

$$R = \frac{L}{2\pi}. \tag{4}$$

Dimensionless arclength s, dimensionless curvature c and dimensionless pressure p take on the respective forms

$$s = \frac{S}{R}, \qquad c = CR, \qquad p = \frac{PR^3}{k_c}. \tag{5}$$

The enclosed area is normalized with respect to the maximal possible enclosed area A_max

$$a = \frac{A}{A_\mathrm{max}} \tag{6}$$

$$A_\mathrm{max} = \pi R^2$$

and the membrane free energy is normalized with respect to the bending energy of a circle with

$C_0 = 0$, ($W_{\mathrm{b,\,circle}} = k_\mathrm{c}\,\pi/R$):

$$w_b = \frac{1}{2\pi}\int_0^{2\pi} c^2\,\mathrm{d}s. \tag{7}$$

Minimization of the dimensionless membrane free energy was performed by variation of the free energy $\delta F = 0$. The constraints requiring fixed curve perimeter

$$1 = \int_0^1 \mathrm{d}s \tag{8}$$

and fixed enclosed area

$$a = \int_0^1 x(s)\sin\Psi(s)\,\mathrm{d}s \tag{9}$$

were taken into account.

The dimensionless area can take on values within the interval $a \in [0,1]$, with 1 corresponding to a circle. The variational problem was solved using Euler-Lagrange formalism, which yielded four coupled differential equations

$$\ddot{\Psi}(s) - px(s)\cos\Psi(s) - \kappa(s)\sin\Psi(s) = 0,$$

$$\dot{x}(s) - \cos\Psi(s) = 0, \quad \dot{y}(s) + \sin\Psi(s) = 0,$$

$$\dot{\kappa}(s) - p\sin\Psi(s) = 0, \tag{10}$$

where $x(s)$ and $y(s)$ denote the plane coordinates and $\kappa(s)$ is a local Lagrange multiplier. The equations were solved numerically by the shooting method. Mathematica, Wolfram Reserch, Inc. (version 9.0.1.0, Champaign, U.S.A.) was used for calculation. Some results were further rendered by Surface Evolver, an open-source software (version 2.70, Susquehanna, U.S.A.), available at http://www.susqu.edu/brakke/evolver/evolver.html.

Results

Figure 2 shows the effect of CB on washed erythrocytes (A) and platelets (B) as observed by the scanning electron microscope (SEM). Erythrocytes and platelets were incubated with CB nanomaterial for 1 hour. Most of the cells in Figure 2A reveal discocytic shape (short arrow). Deposited material can be seen on the erythrocyte surface that could correspond to CB agglomerates (long arrow). Agglomerates adhered to the erythrocyte surface but did not cause distortion of local membrane curvature. Incubation of platelets with CB nanomaterial preserved the disc-like shape chacteristic for resting platelets (Figure 2B).

The effect of CB nanomaterial on populations of erythrocytes in PBS-diluted blood samples is shown in Figures 3 and 4. Discocytes (Figure 3B, black triangle), echinocytes (Figure 3B, white arrow), spherically shaped cells (Figure 3C, white arrow) and ghosts (Figure 3C, black/white striped arrows) can be distinguished. The contrast in Figure 3C was enhanced to make the ghosts visible.

The number of cells in the test sample and in the control sample diminished with time (Figure 3, Figure 4A), the effect being stronger in control. The differences between the average values of the number of erythrocytes in the frame after 1 hour, 3 hours and 24 hours were statistically significant with sufficient power ($p<10^{-4}$, $P(\alpha=p) > 0.95$). After 1 hour, the control sample contained a higher proportion of echinocytes than the test sample (Figure 4B). No trend for an increase or a decrease of the average proportions of the respective cell types in the test and in the control with time (Figure 4 B,C,D) was observed.

These results indicate that the osmotic effects took place during the observed transformations. As these effects took place also in the control sample, a possible explanation would be that the osmotically active particles were removed from the outer solution by adhering to the glass of the observation chamber and/or by interacting with each other. To attain the Donnan equilibrium, water entered the cells and induced a shape transformation towards the sphere. As the cell membrane poorly tolerates stretching, the continuation of this process caused membrane disintegration and ghost formation. The process took place gradually with time. In the test sample, the added CB nanomaterial changed the osmolarity of the solution in a way to suppress the above process. Nanoparticles increased the osmolarity of the solution by intervening with the adhesion of solutes to the glass and/or with their mutual interaction. Osmotic swelling of cells was therefore decelerated with respect to the control sample.

The theoretically calculated sequence illustrates the suggested mechanism. Figure 5 shows two sequences of calculated two dimensional shapes simulating erythrocyte swelling, starting from a discocyte (a) and an echinocyte (d). Swelling was simulated by increasing the area enclosed by the curve. Initial echinocytic shape had higher energy than the discocytic shape, but increasing the enclosed area diminished the energies and led both sequences to the final circular shape. Thus, the two sequences presented in Figure 5 correspond to two branches in the phase diagram trajectories.

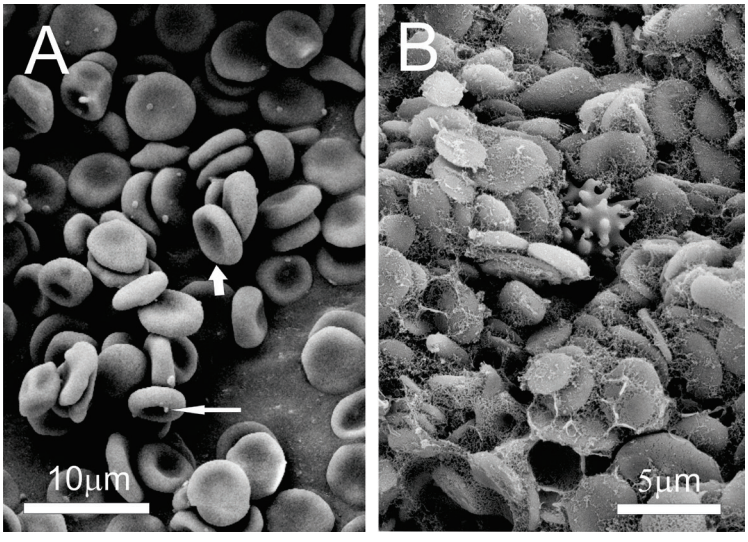

Figure 2: Scanning electron microscope (SEM) images of canine erythrocytes (A) and platelets (B) incubated with carbon black for 1 hour. Carbon black agglomerates adhered to the erythrocyte surface (long arrow) but the normal discoid shape of erythrocytes was preserved (short arrow). Platelets incubated with carbon black for 1 hour retained disc-like shape

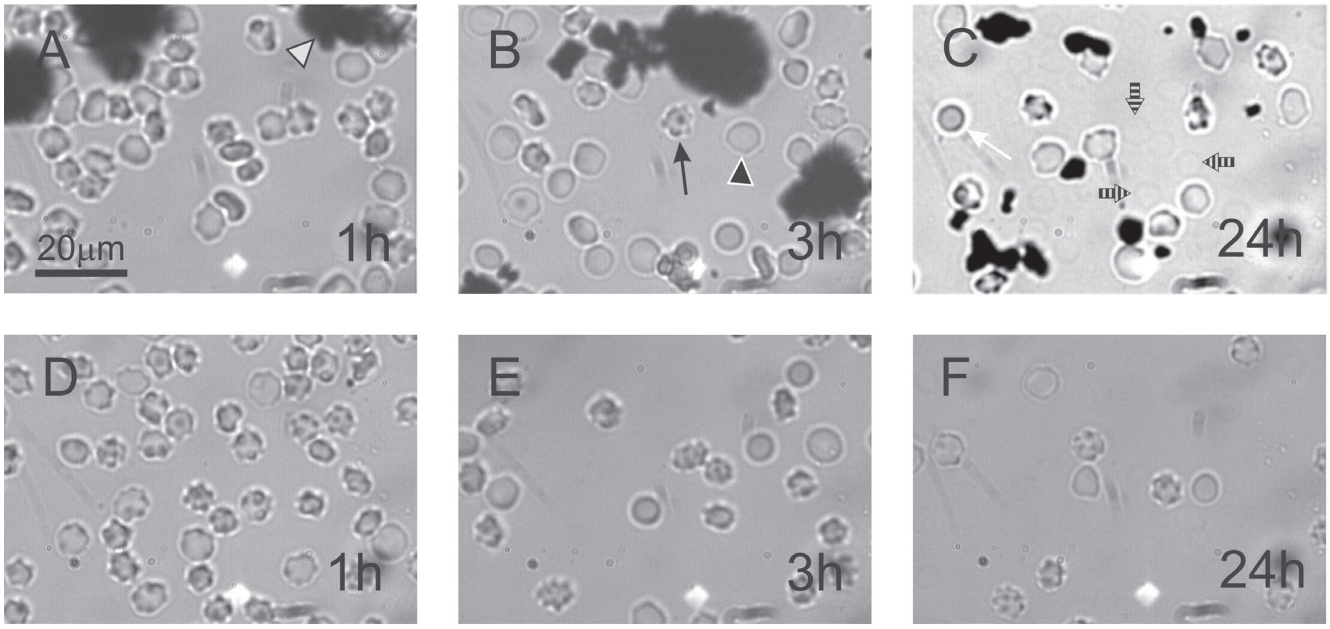

Figure 3: Optical microscope images of populations of PBS-diluted canine blood incubated with carbon black (A-C) after 1 hour, 3 hours and 24 hours, respectively and control samples of PBS-diluted canine blood (D-F) after 1 hour, 3 hours and 24 hours, respectively. Characteristic shapes of erythrocytes: discocytes (B, black triangle), echinocytes (B, black arrow), spherically shaped cells (C, white arrow) and ghosts (C, black/white striped arrows) can be distinguished. White triangle points to a large carbon black aggolmerate (panel A). Contrast in panel C was enhanced to make the ghosts visible

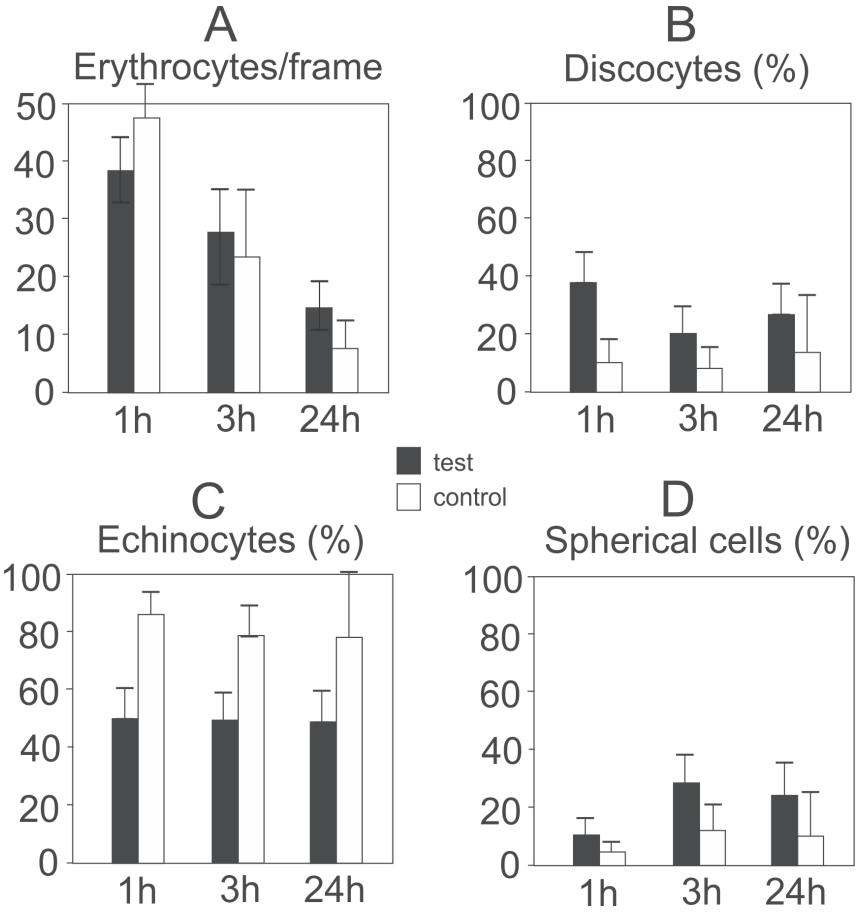

Figure 4: Abundance of erythrocytes with different shape types in the diluted canine blood. A: time dependence of the number of erythrocytes in the test sample and in the control sample, B: portion of the discocytes in the samples, C: portion of the echinocytes in the samples and D: portion of the spherically shaped cells in the samples. Bars denote standard deviations

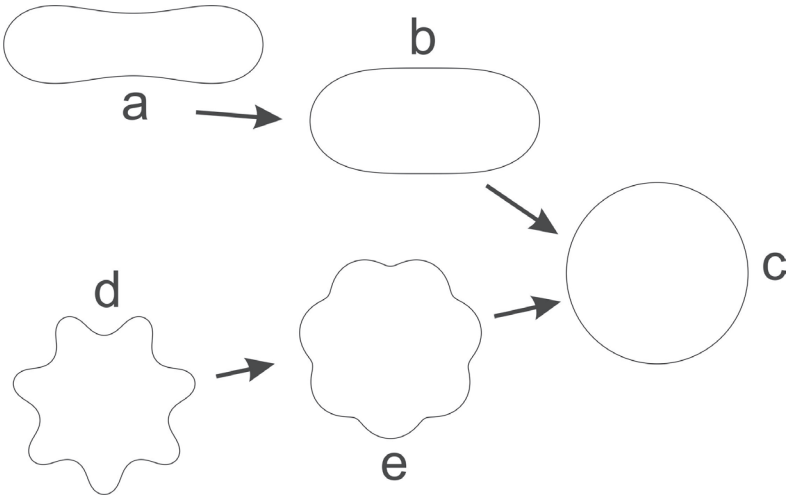

Figure 5: Theoretical description of the osmotic swelling of an erythrocyte starting from a discocyte (a-b-c) and an echinocyte (d-e-c). The shapes were calculated by a two dimensional model based on the minimization of the free energy of the curve at a given enclosed area. The swelling is simulated by an increase of the enclosed area a: 0.57 (shape a), 0.82 (shape b), 1 (shape c), 0.6 (shape d), 0.85 (shape e)

Discussion

In this work, the effect of carbon black nanoparticles on biophysical properties that are revealed in changes of the shape of erythrocytes and platelets was considered. In erythrocytes, haemolytic effects of some types of nanoparticles were reported in the literature (16), where it was suggested that these effects of nanoparticles are due to the shape and size and not the composition of the NPs (16). Toxicity of carbon compounds was found to depend on configuration: nanotubes and quartz were much more toxic than carbon black (28). These effects cannot be explained by the chemical reactions but are related to biophysical mechanisms that were addressed in this work. Namely, shape changes induced by formation of inclusions in membranes lead to membrane budding, vesiculation and finally disintegration.

However, other effects ascribed to nanoparticles were reported in the literature. Production of reactive oxygen species (29), procoagulant activity (30), genotoxicity (31), and effects of biodistribution within the body (32) were reported in leukocytes. Carbon black nanoparticles were found to induce reactive oxygen species-mediated inflammatory effects in bronchial epithelial cell line; the effect correlated with the concentration of nanoparticles and the structure of their surface (33). Furthermore, nanoparticles were found to interact with plasma proteins causing changes in conformation, activation, and inhibition of plasma proteins, exposure of epitopes and changes in physicochemical properties of nanoparticles such as their ability to agglomerate or adsorb proteins (34-35), which influences the coagulation system (36). These effects may depend on time of incubation and amount of nanomaterial (34-35).

We found that CB NPs agglomerated in citrated and phosphate buffered saline and in platelet rich plasma. As regards the biophysical properties that affect the cell shape, no deleterious effects of CB on canine erythrocyte and platelet membranes were observed. Scanning electron micrographs showed that larger CB agglomerates adhered to the erythrocyte membrane but did not distort the local membrane curvature nor the global cell shape (Figure 2A). A decrease of the number of intact erythrocytes in samples in the time interval of 24 hours was observed in the suspensions of PBS-diluted blood (Figure 4A), however, this effect was present also in the control sample (Figure 4A). The number of cells diminished at the expense of the number of ghosts which are poorly visible in the images unless the image is processed (as in Figure 3C). Moreover, spherically shaped cells are present in the samples (Figure 3) indicating that erythrocyte underwent swelling prior to the erythrocyte-ghost transformation. Although the initial number of cells was higher in the control sample (Figure 4A), it decreased more rapidly with time than the number of cells in the test sample, so after 24 hours the number of cells with preserved membrane was considerably and statistically significantly higher in the test sample ($p<10^{-4}$, $P(\alpha=p) > 0.95$).

The theoretical sequences in some aspect illustrate the suggested transformations to sphere derived from the experimental observations, however, the two-dimensional model cannot

describe all the properties of the intermediate shapes.Thus, the extensions of the two dimensional shapes (Figure 5) do not refer to the extensions of the contours of imaged erythrocytes (Figure 3) as the cell volume requires an extension also in the direction perpendicular to the image plane. This is in contrast with the calculated sequence (Figure 5) where the enclosed area increases. It should be kept in mind that the enclosed area of the shapes in Figure 5 represents the cell volume of real cells which increases in osmotic swelling.

In three dimensional models, minimization of the bending energy of laterally isotropic membrane (37) (which is analogous to the expression used in this work) cannot explain the stable shape of the echinocyte but including the shear energy of the membrane skeleton provides a possible explanation (38,39). By using a geometrical ansatz for the shape of the spicules and distributing the spicules over the spherical surface it was found that in the echinocyte – spherical cell transformation the echinocyte spicules become more numerous and thinner when the transformation is driven by an increase of the difference between the outer and the inner membrane layer area (38). A more refined model where the shape of the spicules was determined by a rigorous solution of the variational problem confirmed these results (39). Previous models did not present a rigorous solution to the variational problem for the entire cell which is an advantage of the two dimensional model presented in this work.

Previous theoretical work regarding shape transformation of echinocyte into spherical cell considered mostly processes driven by the change of the difference between the outer and the inner membrane layer areas (40-43). This mechanism takes place if exogeneously added molecules intercalate preferentially in the outer membrane layer (41-43) or due to the conformational change of membrane proteins (44). These results cannot be directly applied to the features considered in our work where the presented two dimesional model provided an illustration of a possible trajectory of shapes in osmotic swelling of initially mildly undulated echinocytes.

CB nanomaterial preserved the disc-like shape of resting platelets (Figure 2B). In contrast, the effect of ZnO nanomaterial was previously found to cause shape transformation of platelets (13). ZnO-treated platelets were considerably rounded and presented tubular protrusions characteristic for activated platelets while CB treated platelets did not exhibit such features. Furthermore, it was previously reported that CB nanoparticles had no effect on the platelet aggregation (26). On the other hand, certain carbon particles stimulated platelet aggregation and accelerated the rate of vascular thrombosis in rat (45).

This study indicates that carbon black nanomaterial may affect blood cells of animal and human indirectly through osmotic effects which were in this study found the most prominent. However, the test sample after 1 hour also contained considerably higher proportion of discocytes than the control sample (Figure 4B) which did not necessary derive from osmotic effects. In order to answer the question whether CB nanomaterial exerts harmful effects on blood cell membranes more refined studies are necessary, including the effect of the integrity of the membrane skeleton (46-48), lateral inhomogeneities of the membrane (49,50), complex interactions between the molecules in the solution (51-53) and microexovesiculation (54) on the cells and their environment.

Conclusions

The effect of CB nanomaterial on the canine erythrocyte membranes was observed. CB agglomerates adhered to the erythrocytes but by that did not cause local or global shape change. Observed hemolysis in the in vitro control samples was explained by the osmotic effects. CB nanomaterial suppressed this hemolytic effect which can be explained by its direct and indirect effect on the osmolarity of the solution. Activation of platelets after 1 hour of incubation with CB nanomaterial was not observed. No harmful direct in vitro effect of CB nanomaterial on the erythrocyte and platelet membrane shapes was found on the level of cell populations.

Acknowledgements

Authors acknowledge support from Slovenian Research Agency fund J1-4109, J3-4108 and P3-0388.

1. Yeates DB, Mauderly JL. Inhaled environmental/occupation irritants and allergens: mechanisms of cardiovascular and systemic responses: introduction. Environ Health Persp 2001; 109: 479–81.

2. Oberdorster G, Oberdorster E, Oberdorster J. Nanotoxicology: an emerging discipline evolving from studies of ultrafine particles. Environ Health Persp 2005; 113: 823–39.

3. Colvin V. The potential environmental impact of engineered nanomaterials. Nat Biotechnol 2003; 13: 1166–70.

4. Vermylen J, Nemmar A, Nemery B, Hoylaerts FM. Ambient air pollution and acute myocardial infarction. J Thromb Haemost 2005; 3 :1955–61.

5. Backer LC, Grindem CB, Corbett WT, Cullins L, Hunter JL. Pet dogs as sentinels for environmental contamination. Sci Total Environ 2001; 274: 161–9.

6. Goodarzi M, Azizi S, Koupaei MJ, Moshkelani S. Pathologic findings of anthraco-silicosis in the lungs of one humped camels (*Camelus dromedarius*) and its role in the occurrence of pneumonia. Kafkas Univ Vet Fak Derg 2014; 20: 171–6.

7. Beytut E. Anthracosis in the lungs and associated lymph nodes in sheep and its potential role in the occurrence of pneumonia. Small Ruminant Res 2002; 46:15–21.

8. Curi NHD, Brait CHH, Antoniosi NR, Talamoni SA. Heavy metals in hair of wild canids from the Brazilian Cerrado. Biol Trace Elem Res 2012; 147: 97–102.

9. Reijnders L. Human health hazards of persistent inorganic and carbon nanoparticles. J Mater Sci 2012; 47: 5061–73.

10. Gardiner K, van Tongeren, Harrington M. Respiratory health effects from exposure to carbon black: results of the phase 2 and 3 cross sectional studies in the European carbon black manufacturing industry. Occup Environ Med 2001; 58: 496–503.

11. Ling MP, Chio CP, Chou WC, et al. Assessing the potential exposure risk and control for airborne titanium dioxide and carbon black nanoparticles in the workplace. Environ Sci Pollut R 2011; 18: 877–89.

12. Vattanasit U, Navasumrit P, Khadka MB, et al. Oxidative DNA damage and inflammatory responses in cultured human cells and humans exposed to traffic – related particles. Int J Hyg Environ Health 2014; 217: 23–33.

13. Šimundić M, Drašler B, Šuštar V, et al. Effect of engineered TiO2 and ZnO nanoparticles on erythrocytes, platelet-rich plasma and giant unilamelar phospholipid vesicles. BMC Vet Res 2013; 9: e7 (13 p) http://www.biomedcentral.com/content/pdf/1746-6148-9-7.pdf

14. Ucciferi N, Collnot EM, Gaiser BK, et al. In vitro toxicological screening of nanoparticles on primary human endothelial cells and the role of flow in odulating cell response. Nanotoxicology 2013; 8: 697–708.

15. Ema M, Naya M, Horimoto M, Kato H. Developmental toxicity of diesel exhaust: a review of studies in experimental animals. Reprod Toxicol 2013; 42: 1–17.

16. Mocan T. Hemolysis as expression of nanoparticles-induced cytotoxicity in red blood cells. Biotechnol Mol Biol Nanomed BMBN 2013; 1(1): 7–12.

17. Van Vliet E. Current standing and future prospects for the technologies proposed to transform toxicity testing in the 21st century. ALTEX 2011; 28: 17–44.

18. Canham PB. The minimum energy of bending as a possible explanation of the biconcave shape of the human red blood cell. J Theor Biol 1970; 26: 61–81.

19. Seifert U. Configurations of fluid membranes and vesicles. Adv Phys 1997; 46:13–137.

20. Gorbet MB, Sefton MV. Biomaterial-associated thrombosis: roles of coagulation factors, complement, platelets and leukocytes-rewiev. Biomaterials 2004; 25: 5681–703.

21. Suwalsky M, Villena F, Norris B, et al. Structural effects of titanium citrate on the human erythrocyte membrane. J Inorg Biochem 2005; 99:764–70.

22. Suwalsky M, Novoa V, Villena F, et al. Structural effects of Zn (2+) on cell membranes and molecular models. J Inorg Biochem 2009; 103:797–804.

23. Suwalsky M, Hernandez P. Aluminum enhances the toxic effects of amyloid beta-peptide on cell membranes and a molecular model. Monatsh Chem 2011; 142: 431–7.

24. Rothen - Rutishauser BM, Schurch S, Haenni B, Kapp N, Gehr P. Interaction of fine particles and nanoparticles with red blood cells visualized with advanced microscopic techniques. Environ Sci Technol 2006; 40: 4353–9.

25. Solomon A, Smyth E, Mitha N, et al. Induction of platelet aggregation after a direct physical interaction with diesel exhaust particles. J

Thromb Heamost 2013; 11: 325–34.

26. Drašler B, Drobne D, Novak S, et al. Effects of magnetic cobalt ferrite nanoparticles on biological and artificial lipid membranes. Int J Nanomed 2014; 9: 1559–81.

27. Šuštar V, Bedina - Zavec A, Štukelj R, et al. Nanoparticles isolated from blood: a reflection of vesiculability of blood cells during the isolation process. Int J Nanomed 2011;6: 2737–48.

28. Tsuji JS, Maynard AD, Howard, et al. Research strategies for safety evaluation of nanomaterials. Part IV: Risk assessment of nanoparticles. Toxicol Sci 2005; 89: 42–50.

29. Piryazev AP, Azizova OA, Aseichev AV, Dudnik LB, Sergienko VI. Effect of gold nanoparticles on production of reactive oxygen species by human peripheral blood leukocytes stimulated with opsonized zymosan. Bull Exp Biol Med 2013; 156: 101–3.

30. Dobrovolskaia MA, Patri AK, Potter TM, Rodriguez JC, Hall JB, McNeil SE.Dendrimer-induced leukocyte procoagulant activity depends on particle size and surface charge. Nanomedicine 2012; *7*: 245–56.

31. Colognato R, Bonelli A, Ponti J, Farina M, Bergaaschi E, Sabbioni E, Migliore L. Comparative genotoxicity of cobalt nanoparticles and ions on human peripheral leukocytes in vitro. Mutagenesis 2008; 23: 377–82.

32. Aggarwal P, Hall JB, McLeland CB, Dobrovolskaia MA, McNeil SE. Nanoparticle interaction with plasma proteins as it relates to particle biodistribution, biocompatibility and therapeutic efficacy. Adv Drug Deliv Rev 2009; 61: 428–37.

33. Hussain S, Boland S, Baeza-Squiban A, et al. Oxidative stress and proinflammatory effects of carbon black and titanium dioxide nanoparticles: role of particle surface area and internalized amount. Toxicology 2009; 260: 142–9.

34. Tsai DH, DelRio FW, Keene AM, et al. Adsorption and conformation of serum albumin protein on gold nanoparticles investigated using dimensional measurements and in situ spectroscopic methods. Langmuir 2011; 27: 2464–77.

35. Izak-Nau E, Voetz M, Eiden S, Duschl A, Puntes VF. Altered characteristics of silica nanoparticles in bovine and human serum: the importance of nanomaterial characterization prior to its toxicological evaluation. Part Fibre Toxicol 2013; 10: e56 (12 p.) http://www.particleandfibretoxicology.com/content/pdf/1743-8977-10-56.pdf

36. Ilinskaya AN, Dobrovolskaia MA. Nanoparticles and the blood coagulation system. Part II: safety concerns. Nanomedicine (Lond) 2013; 8: 969–81.

37. Deuling HJ, Helfrich W. The curvature elasticity of fluid membranes: a catalogue of vesicle shapes. J Phys 1976; 37: 1335–45.

38. Iglič A. A possible mechanism determining the stability of spiculated red blood cells. J Biomech 1997; 30: 35–40.

39. Mukhopadhyay R, Lim HWG, Wortis M. Echinocyte shapes: bending, stretching, and shear determine spicule shape and spacing. Biophys J 2002; 82:1756–72.

40. Sheetz MP, Singer SJ. Biological membranes as bilayer couples: a molecular mechanism of drug-erythrocyte interactions. Proc Natl Acad Sci 1974; 71: 4457–4461.

41. Iglič A, Kralj - Iglič V, Hägerstrand H. Amphiphile induced echinocyte-spheroechinocyte red blood cell shape transformation. Eur Biophys J 1998; 27: 335–9.

42. Iglič A, Kralj-Iglič V, Hägerstrand H. Stability of spiculated red blood cells induced by intercalation of amphiphiles in cell membrane. Med Biol Eng Comput 1998; 36: 251–5.

43. Iglič A, Hägerstand H. Amphiphile-induced spherical microexovesicle corresponds to an extreme local area difference between two monolayers of the membrane bilayer. Med Biol Eng Comp 1999; 37: 125–9.

44. Gimsa J, Ried C. Do band 3 protein conformational changes mediate shape changes of human erythrocytes? Mol Membr Biol 1995; 12: 247–54.

45. Radomski A, Jurasz P, Alonso - Escolano D, et al. Nanoparticle-induced platelet aggregation and vascular thrombosis. Br J Pharmacol 2005; 146: 882–93.

46. Bobrowska - Hägerstrand M, Hägerstrand H, Iglič A. Membrane skeleton and red blood cell vesiculation at low pH. Biochim Biophys Acta 1998; 1371: 123–8.

47. Hägerstrand H, Danieluk M, Bobrowska Hägerstrand M, et al. Influence of band 3 protein absence and skeletal structures on amphiphile- and Ca^{2+}-induced shape alterations in erythrocytes: a study with lamprey (*Lampetra fluviatilis*), trout (*Onchorhynchus mykiss*) and human erythrocytes. BBA Biomembranes 2000; 1466, 125–38.

48. Hianik T, Rybár P, Bernhardt I. Adiabatic compressibility of red blood cell membrane: in-

fluence of skeleton. Bioelectrochemistry 2000; 52: 197–201.

49. Mrówczyńska L, Salzer U, Iglič A, Hägerstrand H. Curvature factor and membrane solubilization, with particular reference to membrane rafts. Cell Biol Int 2011; 35: 991–5.

50. Mrówczyńska L, Salzer U, Perutková Š, Iglič A, Hägerstrand H. Echinophilic proteins stomatin, sorcin, and synexin locate outside ganglioside M1 (GM1) patches in the erythrocyte membrane. Biochem Biophys Res Commun 2010; 401: 396–400.

51. Mrówczyńska L, Bielawski J. The mechanism of bile salt-induced hemolysis. Cell Mol Biol Lett 2001; 6: 881–95.

52. Jasiewicz B, Mrówczyńska L, Malczewska-Jaskola K. Synthesis and haemolytic activity of novel salts made of nicotine alkaloids and bile avids. Bioorg Med Chem Lett 2014; 24: 1104–7.

53. Rudenko S V. Erythrocyte morphological states, phases, transitions and trajectories. Biochim Biophys Acta 2010; 1798: 1767–78.

54. Mrvar - Brečko A, Šuštar V, Janša V, et al. Isolated microvesicles from peripheral blood and body fluids as observed by scanning electron microscope. Blood Cells Mol Dis 2010; 44: 307–12.

VPLIV NANOMATERIALA ČRNEGA OGLJIKA NA OBLIKO PASJIH ERITROCITOV IN TROMBOCITOV

J. L. Krek, M. Šimundić, M. Drab, M. Pajnič, V. Šuštar, R. Štukelj, D. Drobne, V. Kralj-Iglič

Povzetek: Obravnavali smo vpliv aglomeriranega nanomateriala črnega ogljika na biofizikalne lastnosti membrane, ki se odražajo v spremembah celične oblike pasjih rdečih krvniček in trombocitov. Vzorce pasje krvi, razredčene s citriranim fosfatnim pufrom, smo inkubirali z nanomaterialom črnega ogljika in jih opazovali z vrstičnim elektronskim mikroskopom ter optičnim mikroskopom. Ugotovili smo, da aglomerati nanomateriala interagirajo z membrano eritrocita. Na populacijah smo opazovali število celic in deleže posameznih vrst celic glede na obliko (diskociti, ehinociti, kroglaste celice) v suspenziji z dodanim nanomaterialom črnega ogljika in v kontrolni suspenziji z dodanim citriranim fosfatnim pufrom. Kolektive, oblikovane iz reprezentativnih slik populacij celic, smo ocenili s statističnimi metodami. Za lažjo ponazoritev procesa osmotskega nabrekanja eritrocita iz začetne diskocitne ali ehinocitne v končno kroglasto obliko, ki ji sledi disintegracija membrane, smo izdelali dvodimenzionalni matematični model oblike eritrocita. V razredčeni krvi smo našli aglomerate nanomateriala črnega ogljika z največjo razsežnostjo v mikrometrskem območju. Aglomerati so interagirali z membrano eritrocita, ne da bi opazno spremenili lokalno ukrivljenost membrane in obliko celotne celice. Inkubacija krvi s citriranim fosfatnim pufrom je povzročila časovno odvisno zmanjševanje števila intaktnih eritrocitov v vzorcih, kar smo pripisali disintegraciji membrane eritrocita, pri čemer pa je dodan nanomaterial črnega ogljika deloval zaviralno. Relativni deleži posameznih vrst oblik so se v 24 urah v veliki meri ohranili. Opažene pojave smo lahko razložili z osmotskimi učinki. Inkubacija pasjih trombocitov z nanomaterialom črnega ogljika je v 24 urah ohranila diskasto obliko, ki je značilna za mirujoče trombocite. Ugotovili smo, da nanomaterial črnega ogljika interagira z membrano krvnih celic, vendar nima neposrednega učinka na lokalno in globalno obliko celice. Veliki aglomerati, ki nastanejo v krvni plazmi, pa bi lahko predstavljali mehanske ovire v krvnem obtoku.

Ključne besede: črni ogljik; nanodelci; oblika eritrocita; osmoza; varnost nanomaterialov; nanotoksikologija; alternativa laboratorijskim/poskusnim živalim